

Loading FeOOH on Ni(OH)₂ hollow nanorods to obtain a three-dimensional sandwich catalyst with strong electron interactions for efficient oxygen-evolution reaction

Wenjun Guo,^{ab} Dandan Li,^{ab} Dazhong Zhong,^{ab} Shuai Chen,^c Genyan Hao,^{ab} Guang Liu,^{ab} Jinping Li^{ab} and Qiang Zhao^{* ab}

^aResearch Institute of Special Chemicals, Taiyuan University of Technology, Taiyuan 030024, Shanxi, P.R. China.

^bShanxi Key Laboratory of Gas Energy Efficient and Clean Utilization, Taiyuan 030024, Shanxi, P.R. China.

^cState Key Laboratory of Coal Conversion, Institute of Coal Chemistry, Chinese Academy of Science, Taiyuan 030001, Shanxi, P. R. China.

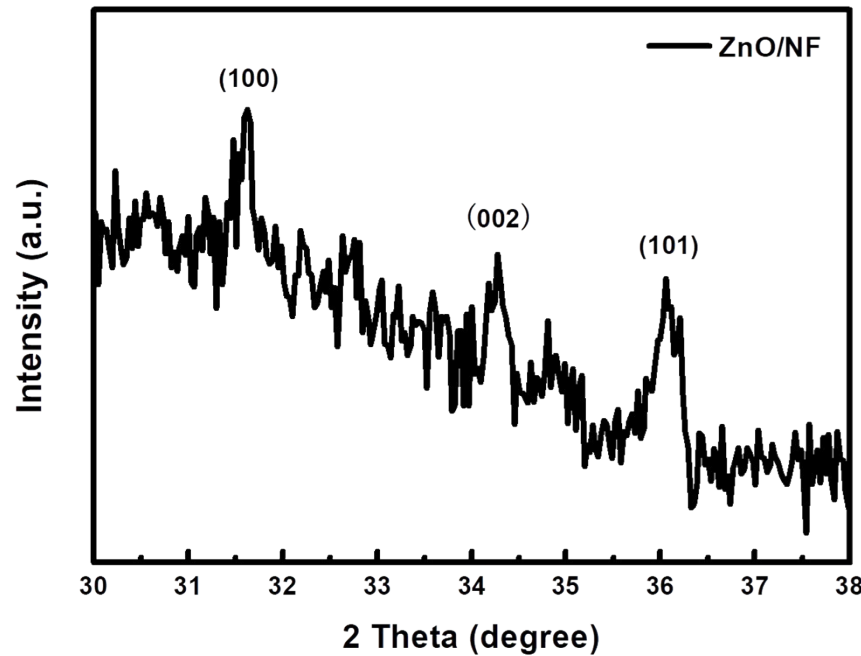


Figure S1. XRD pattern of ZnO.

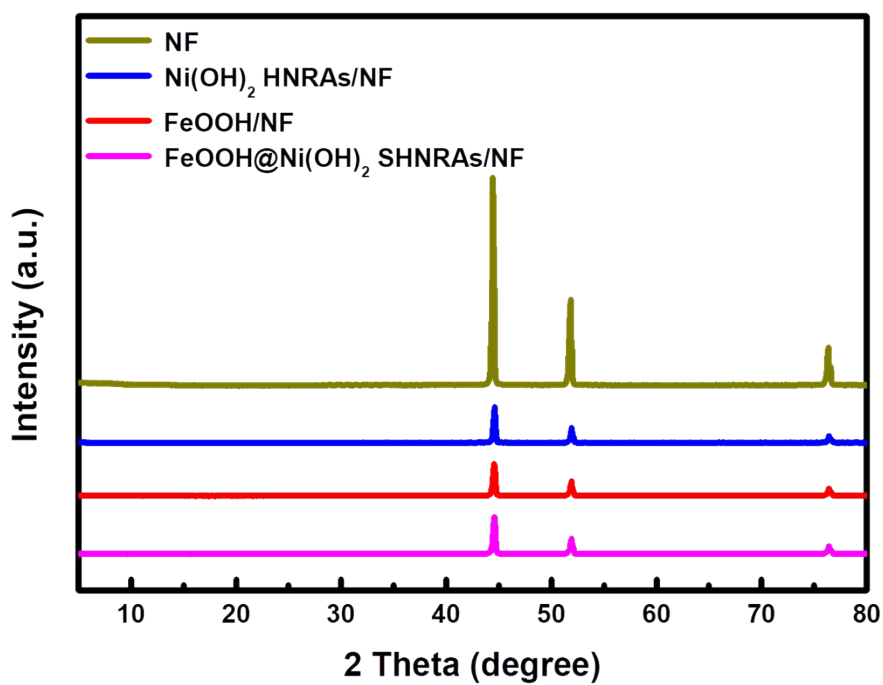


Figure S2. XRD patterns of NF, Ni(OH)_2 HNRAs/NF, FeOOH/NF and FeOOH@Ni(OH)_2 SHNRAs/NF.

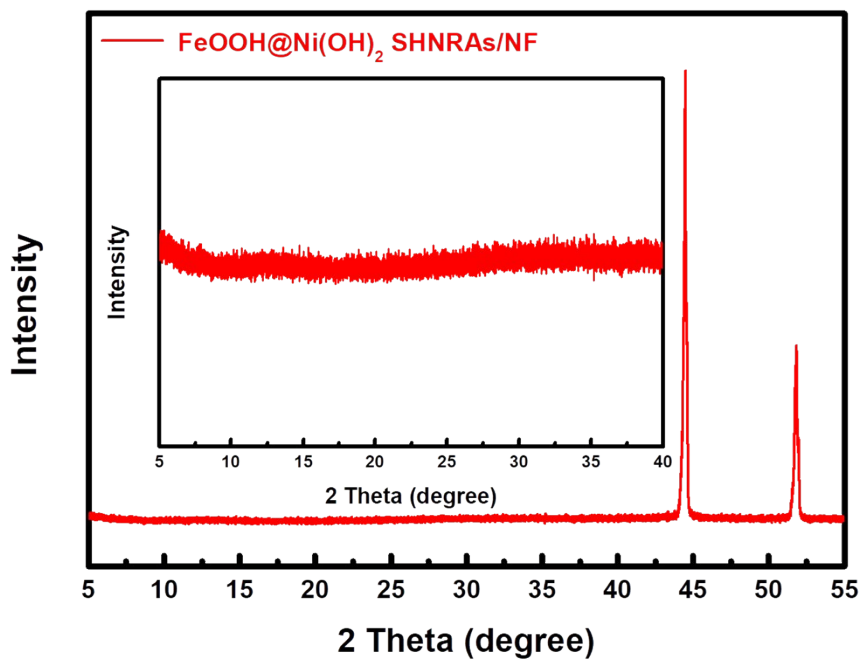


Figure S3. XRD pattern of FeOOH@Ni(OH)_2 SHNRAs/NF by slow scanning for 1 h.

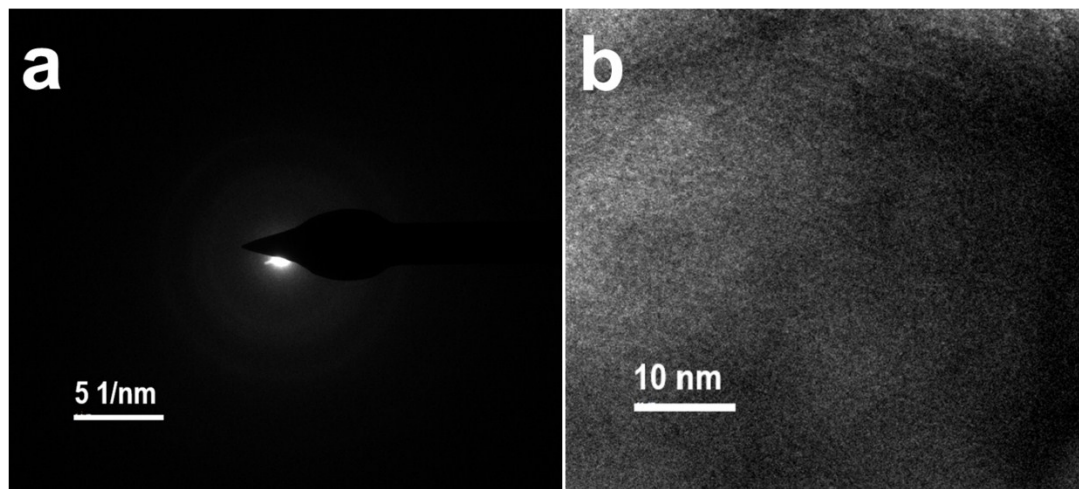


Figure S4. (a) SAED pattern of $\text{Ni}(\text{OH})_2$ HNRAs/NF, (b) High-resolution TEM image of $\text{Ni}(\text{OH})_2$ HNRAs/NF.

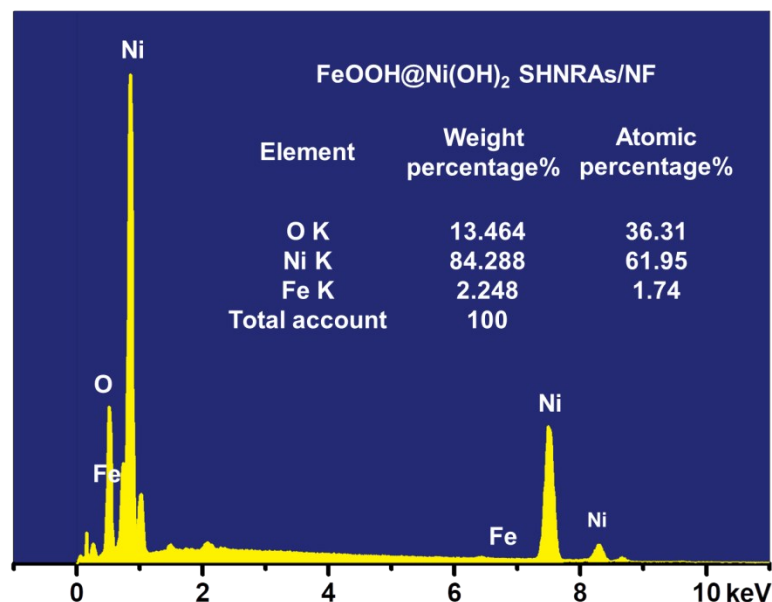


Figure S5. EDS profile of $\text{FeOOH}@\text{Ni}(\text{OH})_2$ SHNRAs/NF.

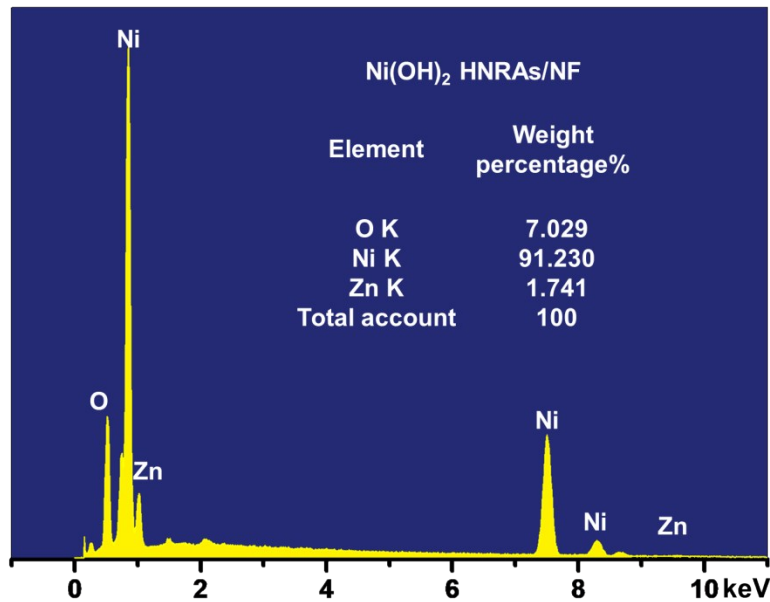


Figure S6. EDS profile of Ni(OH)₂ HNRAs/NF.

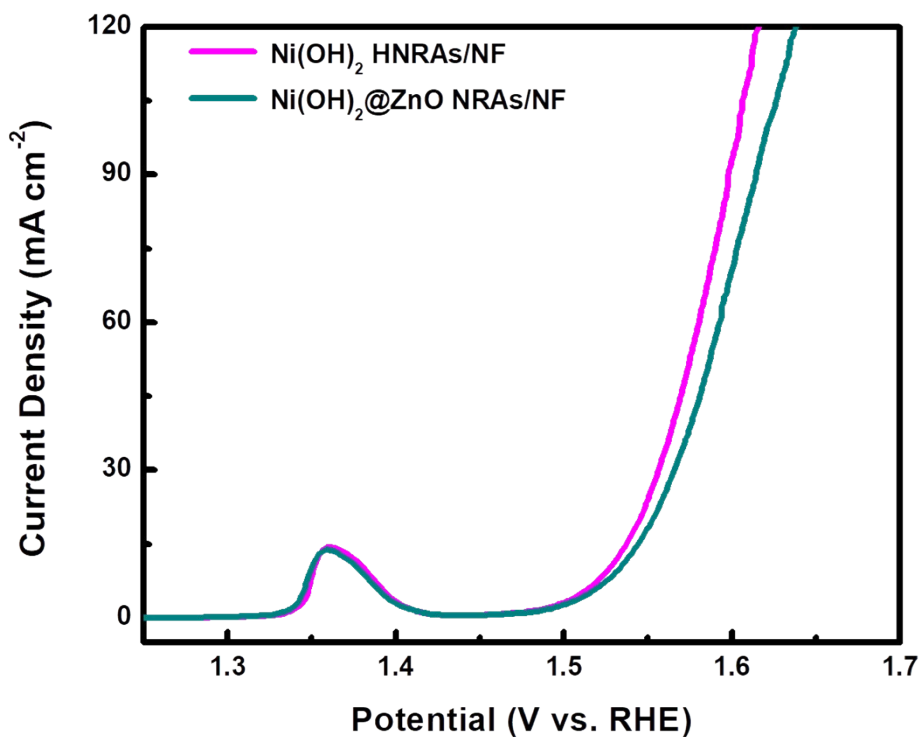


Figure S7. Effect of ZnO template on electrochemical performance of Ni(OH)₂ catalyst.

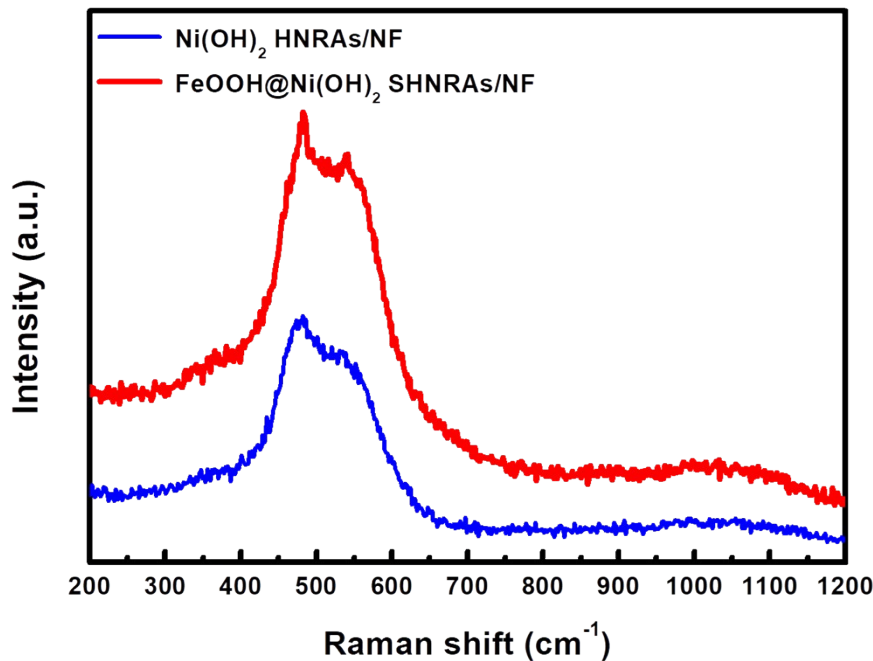


Figure S8. Raman spectra of Ni(OH)_2 HNRAs/NF and $\text{FeOOH}@\text{Ni(OH)}_2$ SHNRAs/NF.

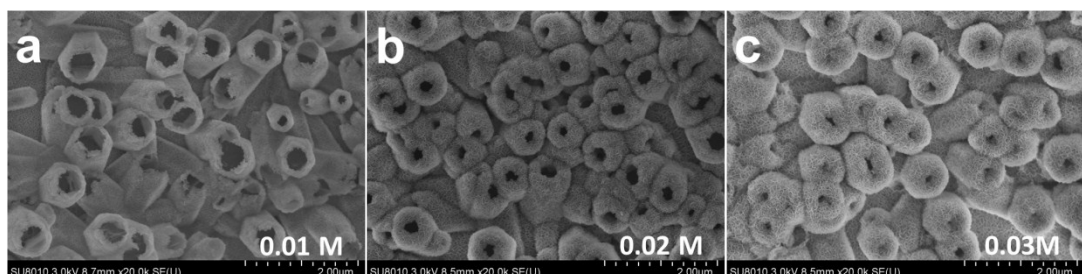


Figure S9. Effect of Ni concentration on the morphology of Ni(OH)_2 HNRAs/NF:
SEM images of (a) 0.01M, (b) 0.02M, (c) 0.03M.

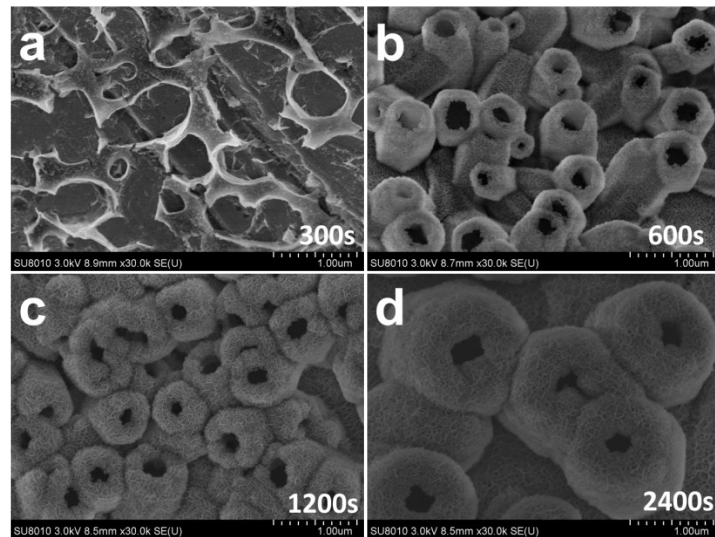


Figure S10. Effect of Ni deposition time on the morphology of $\text{Ni}(\text{OH})_2$ HNRAs/NF:
SEM images of (a) 300s, (b) 600s, (c) 1200s, (d) 2400s.

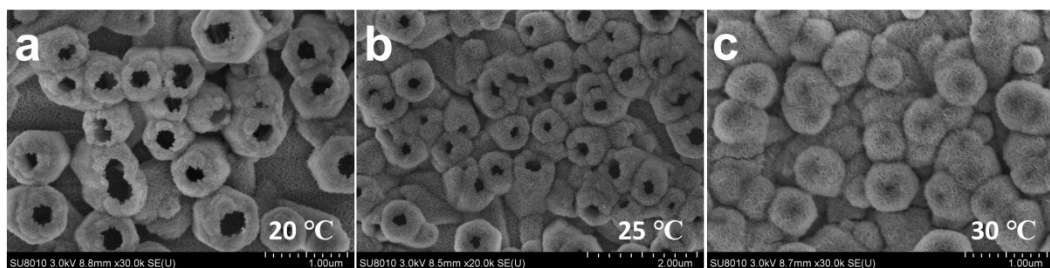


Figure S11. Effect of Ni deposition temperature on the morphology of $\text{Ni}(\text{OH})_2$
HNRAs/NF: SEM images of (a) 20°C, (b) 25°C, (c) 30°C.

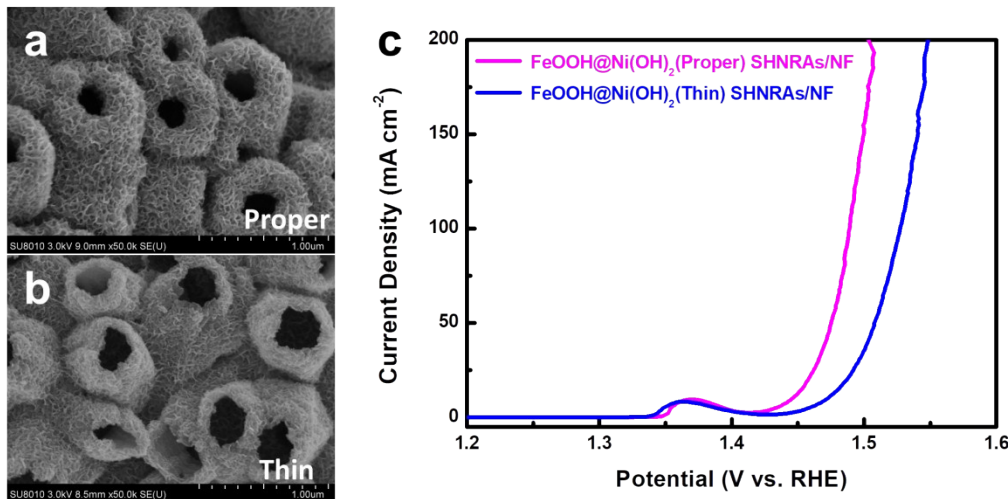


Figure S12. SEM image of (a) $\text{FeOOH}@\text{Ni}(\text{OH})_2$ (Proper) SHNRAs/NF, (b)
 $\text{FeOOH}@\text{Ni}(\text{OH})_2$ (Thin) SHNRAs/NF, (c) Polarization curves (iR-compensated) of
them.

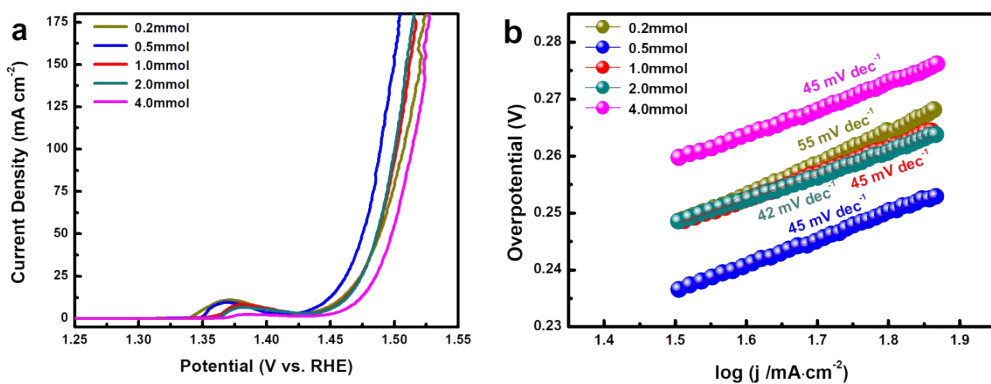


Figure S13. Effect of Fe concentration on electrochemical performance of FeOOH@Ni(OH)₂ SHNRAs/NF: (a) Polarization curves (iR-compensated), (b) Tafel slopes.

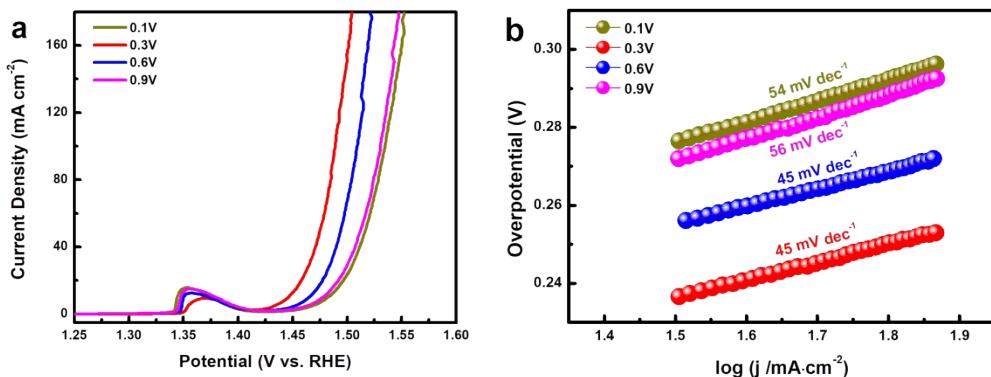


Figure S14. Effect of Fe deposition voltage on electrochemical performance of FeOOH@Ni(OH)₂ SHNRAs/NF: (a) Polarization curves (iR-compensated), (b) Tafel slopes.

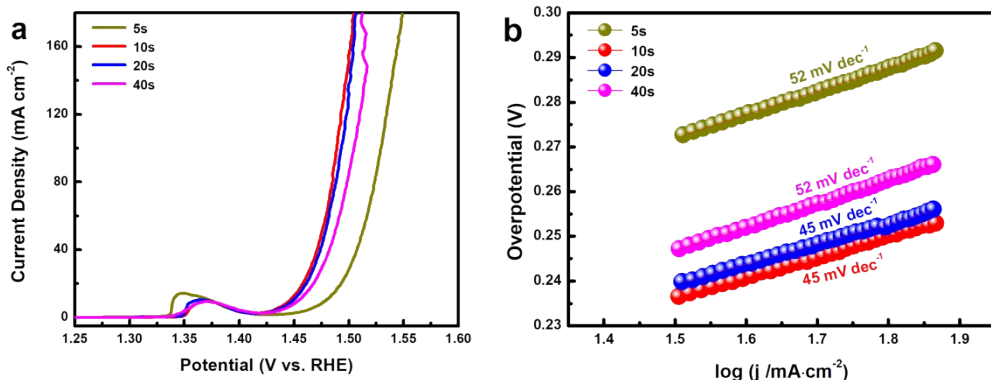


Figure S15. Effect of Fe deposition time on electrochemical performance of FeOOH@Ni(OH)₂ SHNRAs/NF: (a) Polarization curves (iR-compensated), (b) Tafel

slopes.

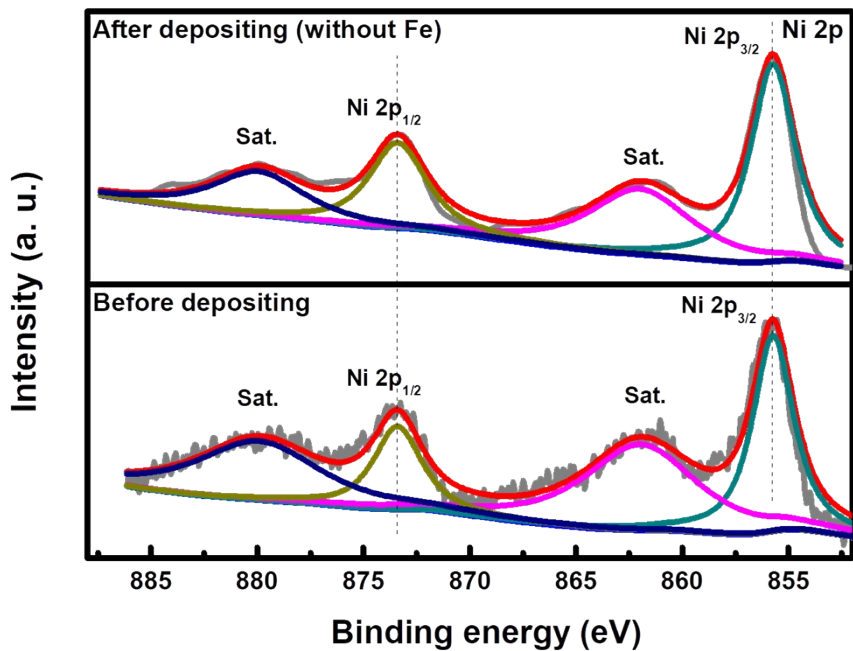


Figure S16. XPS spectra of Ni 2p region for $\text{Ni}(\text{OH})_2$ HNRAs/NF before and after electrochemical deposition process.

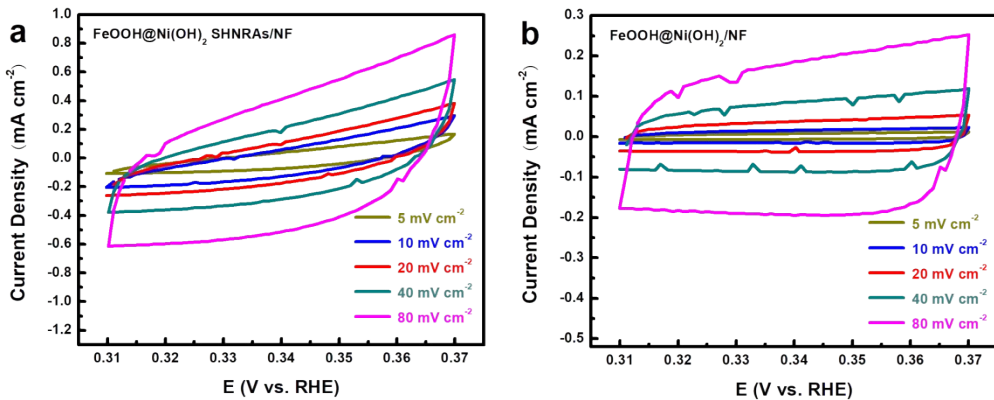


Figure S17. CV curves in a potential range of 0.31–0.37 V versus RHE of (a) $\text{FeOOH@Ni}(\text{OH})_2$ SHNRAs/NF, and (b) $\text{FeOOH@Ni}(\text{OH})_2/\text{NF}$ in 1.0 M KOH.

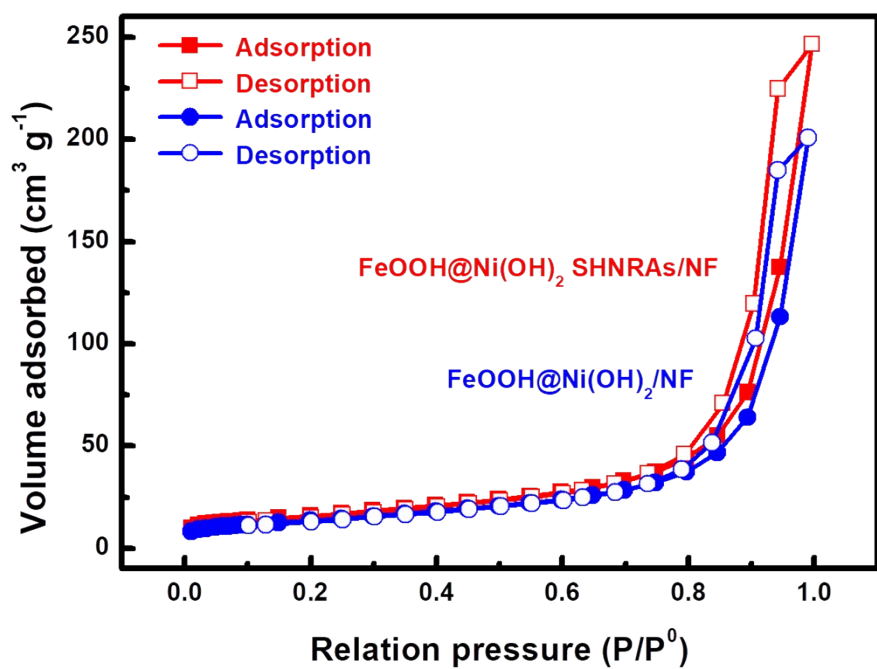


Figure S18. Nitrogen adsorption-desorption isotherms of FeOOH@Ni(OH)₂ SHNRAs and FeOOH@Ni(OH)₂ catalysts.

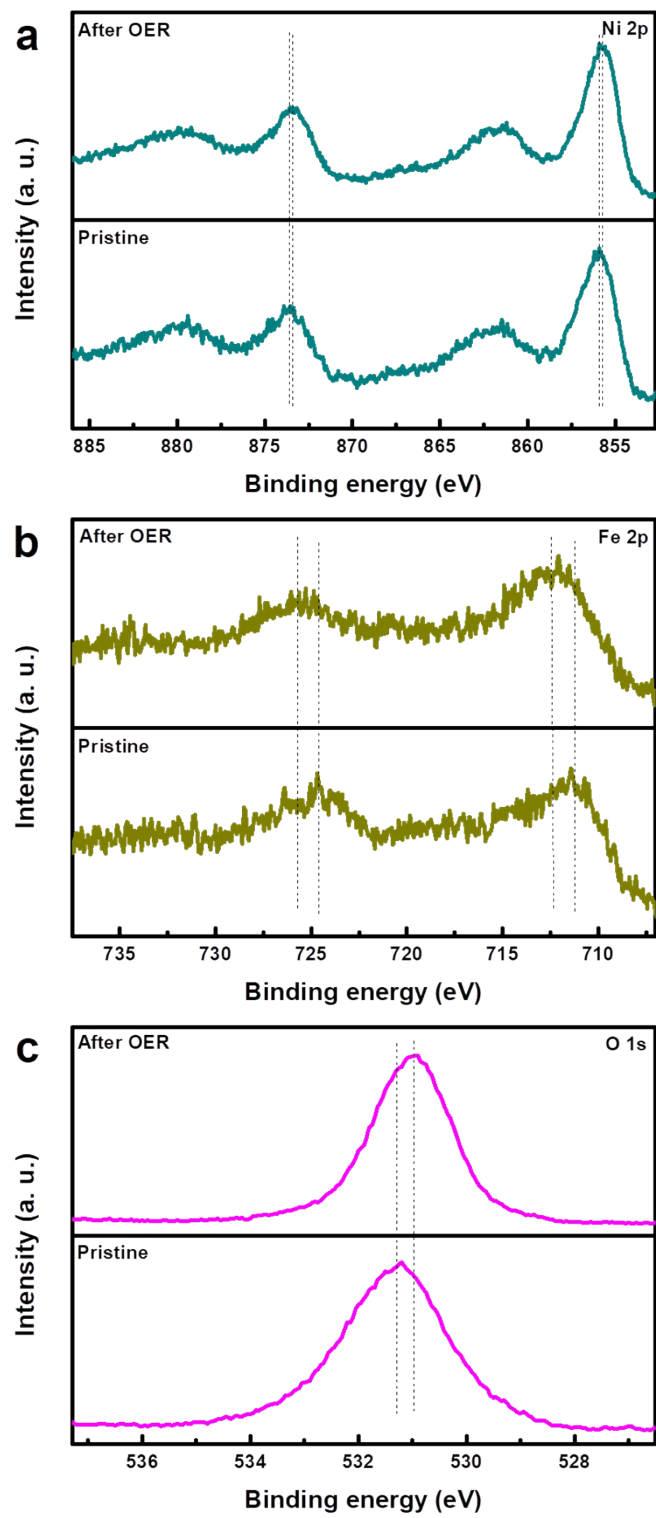


Figure S19. XPS spectra of (a) Ni 2p, (b) Fe 2p and (c) O 1s region for $\text{FeOOH}@\text{Ni(OH)}_2$ SHNRAs/NF before and after OER testing.

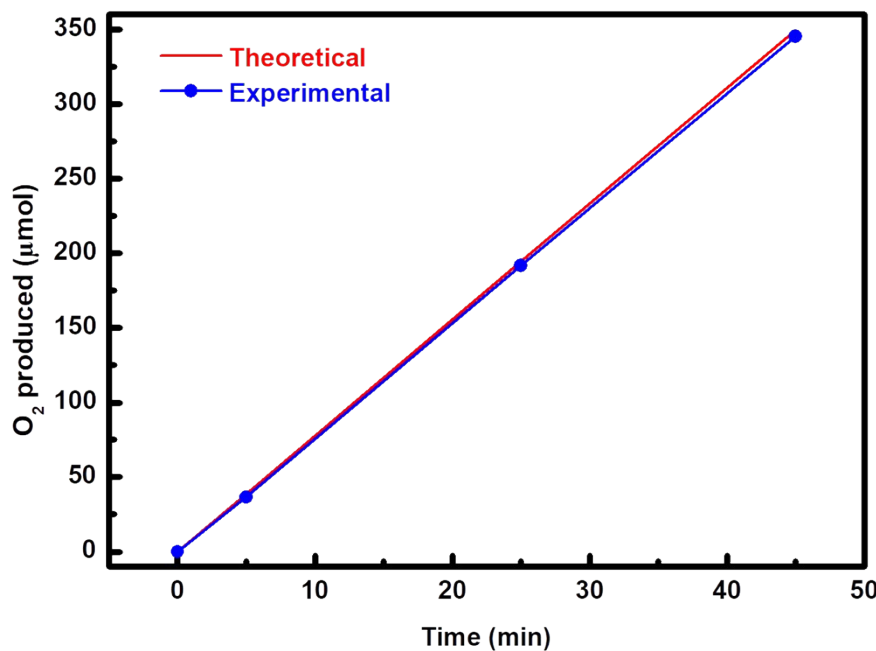


Figure S20. Experimental vs. theoretical amount of O₂ produced using the FeOOH@Ni(OH)₂ SHNRAs/NF electrode at a fixed current of 50 mA.

Table S1. Comparison of catalytic performance with other similar catalysts that have been reported ($\eta@j$: Overpotential at the applied current density)

Catalyst	Electrode substrate	$\eta@j$ /mV	Tafel slope /mV dec ⁻¹	Electrolyte	Reference
FeOOH@Ni(OH)₂ SHNRAs	NF	245@50	45	1 M KOH	This work
NiSe@NiOOH	NF	332@50	162	1 M KOH	[1]
Ni ₃₂ Fe oxide	NF	291@10	58	1 M KOH	[2]
Fe(0.5)-doped β-Ni(OH) ₂	RDE	260@10	32	1 M KOH	[3]
S-NiFe ₂ O ₄	NF	267@10	36.7	1 M KOH	[4]
Fe _{11%} -NiO	NF	259@50	49.4	1 M KOH	[5]
NiCoFe _x P	CC	290@100	56	1 M KOH	[6]
FeOOH/NiFe LDH	NF	330@100	-	1 M KOH	[7]
H-NiCoFe LDH	NF	438@30	81	1 M KOH	[8]
NiFe LDH	GC	280@10	49.4	1 M KOH	[9]
NiFe LDH	NF	280@30	50	1 M KOH	[10]

FeOOH nanoparticles	NF	390@10	78.6	0.1 M KOH	[11]
Ni–Fe(O _x H _y)	NF	298@10	37	1 M KOH	[12]
NiFe LDH/NiCo ₂ O ₄	NF	290@50	53	1 M KOH	[13]

References

1. X. Li, G. Q. Han, Y. R. Liu, B. Dong, W. H. Hu, X. Shang, Y. M. Chai and C. G. Liu, *ACS applied materials & interfaces*, 2016, **8**, 20057-20066.
2. M. Yu, G. Moon, E. Bill and H. Tüysüz, *ACS Applied Energy Materials*, 2019, **2**, 1199-1209.
3. K. Zhu, H. Liu, M. Li, X. Li, J. Wang, X. Zhu and W. Yang, *Journal of Materials Chemistry A*, 2017, **5**, 7753-7758.
4. J. Liu, D. Zhu, T. Ling, A. Vasileff and S.-Z. Qiao, *Nano Energy*, 2017, **40**, 264-273.
5. Z. Wu, Z. Zou, J. Huang and F. Gao, *Journal of Catalysis*, 2018, **358**, 243-252.
6. C. Ray, S. C. Lee, B. Jin, A. Kundu, J. H. Park and S. C. Jun, *ACS Sustainable Chemistry & Engineering*, 2018, **6**, 6146-6156.
7. J. Chi, H. Yu, G. Jiang, J. Jia, B. Qin, B. Yi and Z. Shao, *Journal of Materials Chemistry A*, 2018, **6**, 3397-3401.
8. Q. Yang, T. Li, Z. Lu, X. Sun and J. Liu, *Nanoscale*, 2014, **6**, 11789-11794.
9. L. Yu, J. F. Yang, B. Y. Guan, Y. Lu and X. W. D. Lou, *Angewandte Chemie*, 2018, **57**, 172-176.
10. Z. Lu, W. Xu, W. Zhu, Q. Yang, X. Lei, J. Liu, Y. Li, X. Sun and X. Duan, *Chemical communications*, 2014, **50**, 6479-6482.
11. J. Lee, H. Lee and B. Lim, *Journal of Industrial and Engineering Chemistry*, 2018, **58**, 100-104.
12. M. Gorlin, P. Chernev, P. Paciok, C. W. Tai, J. Ferreira de Araujo, T. Reier, M. Heggen, R. Dunin-Borkowski, P. Strasser and H. Dau, *Chemical communications*, 2019, **55**, 818-821.
13. Z. Wang, S. Zeng, W. Liu, X. Wang, Q. Li, Z. Zhao and F. Geng, *ACS applied materials & interfaces*, 2017, **9**, 1488-1495.